Proceedings of the Twenty-ninth (2019) International Ocean and Polar Engineering Conference **www.isope.org**
Honolulu, Hawaii, USA, June 16-21, 2019

ISBN 978-1 880653 85-2; ISSN 1098-6189

A Continuum Poroelastic Model for Gravity Waves on an Ice-Covered Ocean

Hua Chen, Robert P. Gilbert, Philippe Guyenne
Department of Mathematical Sciences, University of Delaware, Newark, DE, USA

ABSTRACT

The recurrent interactions between ocean waves and sea ice are a widespread feature of the polar regions, and their impact on sea-ice dynamics and morphology has been increasingly recognized as evidenced by the surge of research activity during the last two decades. The rapid decline of summer ice extent that has occurred in the Arctic Ocean over recent years has contributed to the renewed interest in this subject. Continuum models have recently gained popularity to describe wave propagation in various types of ice cover and across a wide range of length scales. In this paper, we propose a continuum wave-ice model where the floating sea ice is described as a homogeneous poroelastic material and the underlying ocean is viewed as a slightly compressible fluid. The exact dispersion relation for linear traveling wave solutions of this coupled system is established and compared to predictions from existing theories.

KEY WORDS: Gravity waves; porous material; viscoelasticity; wave attenuation; wave scattering; wave-ice interactions.

INTRODUCTION

Wave-ice interaction is a two-way process. Ice scatters ocean waves and redistributes wave energy, in turn gravity waves stress and potentially fracture ice. In this paper, we focus on the phenomenon of ice-induced wave attenuation (Wadhams et al, 1988). A common place where wave-ice interactions play an important role is the marginal ice zone (MIZ), which is the outer edge of the ice cover, closest to the open ocean. It typically consists of ice floes, brash ice and open water.

Several linear models have been proposed to study wave-ice interactions and can generally be classified into two categories: solitary-floe models and continuum models (Squire, 2007; Kohout and Meylan, 2008). Of special interest here is the latter category. The mass-loading (ML) model is probably the most basic continuum formulation. It treats ice floes as a simple mass load on the ocean surface. The thin elastic plate model (hereafter referred to as FS) incorporates the elastic response of the ice layer into the formulation, with the ice layer being described as a Kirchhoff–Love plate (Fox and Squire, 1994). Alternatively, Keller (1998) proposed a two-layer formulation where a viscous fluid layer lies on top of an ideal fluid region. In this context, viscosity stems from the fact that the ice cover is viewed as a suspension of solid particles in water. Building upon Keller's work, Wang and Shen (2010, now referred to as WS) included elasticity in the upper layer and described the ice layer as a homogeneous incompressible viscoelastic medium according to Voigt's model. Their viscoelastic fluid model synthesizes the thin elastic plate and viscous layer models as limiting cases under suitable conditions. Recently, Mosig et al (2015) extended the FS model by introducing a complex Voigt shear modulus to account for viscous dissipation. This extended model is referred to as EFS in the following sections.

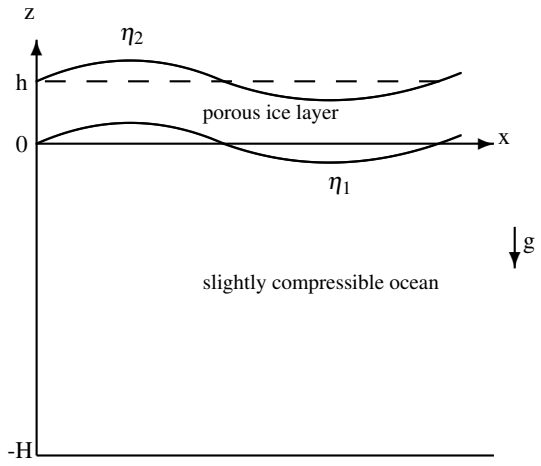

Fig. 1: Sketch of the coupled ice-ocean system.

MATHEMATICAL FORMULATION

In this paper, we consider the two-dimensional setting of linear gravity waves propagating on an ocean of uniform depth H, with an ice layer lying on top of it. We adopt the continuum viewpoint in which a heterogeneous ice field such as in the MIZ may be modeled as a homogeneous medium with effective properties controlled by constant rheological parameters. The x-axis represents the horizontal direction, along which waves propagate. The z-axis points upward and the $z = 0$ level corresponds to the ice-water interface at rest (see Fig. 1). We

assume there is no separation between the ocean and the ice layer. It is also necessary to assume that the ocean fluid has small compressibility to ensure the ocean velocity potential is compatible with solutions of Biot's equations for a poroelastic ice layer (Biot, 1956).

Equations for the Underlying Ocean

It follows from mass and momentum conservation for a slightly compressible fluid that the velocity potential Φ satisfies the wave equation

$$\partial_t^2\Phi - c^2\nabla^2\Phi = 0\,, \quad \text{for} \quad x\in\mathbb{R}\,, -H<z<0\,, \tag{1}$$

where the speed of sound c is given by

$$c^2 = \left.\frac{\partial P}{\partial\rho}\right|_{\rho=\rho_f}\,,$$

in terms of fluid pressure P and fluid density ρ_f, assuming the fluid is isothermal (Renzi and Dias, 2014). The variable t represents time and the symbol $\nabla=(\partial_x,\partial_z)$ stands for the spatial gradient. Let $z=\eta_1(x,t)$ denote the ice-water interface. For gentle deformations, the kinematic condition reads

$$\partial_z\Phi = \partial_t\eta_1\,, \quad \text{at} \quad z=0\,, \tag{2}$$

and Bernoulli's condition takes the form

$$P = -\rho_f(\partial_t\Phi + g\,\eta_1)\,, \quad \text{at} \quad z=0\,. \tag{3}$$

At the ocean floor, the impermeability condition implies

$$\partial_z\Phi = 0\,, \quad \text{at} \quad z=-H\,.$$

Equations for the Floating Sea Ice

The ice layer is viewed as an infinite strip of uniform thickness h lying on top of the ocean and is modeled as a poroelastic material according to Biot's theory. At any point in this material, let $\mathbf{u}=(u,v)$ and $\mathbf{U}=(U,V)$ denote the solid and fluid displacement fields, respectively. The strain tensor associated with the solid part is given by the geometric relations

$$e_{xx}=\partial_x u\,, \quad e_{xz}=e_{zx}=\frac{1}{2}\left(\partial_z u+\partial_x v\right)\,, \quad e_{zz}=\partial_z v\,.$$

The solid and fluid dilatations are defined by

$$\begin{aligned} e &= \nabla\cdot\mathbf{u} = \partial_x u+\partial_z v\,,\\ \varepsilon &= \nabla\cdot\mathbf{U} = \partial_x U+\partial_z V\,, \end{aligned}$$

respectively.

Following Gilbert et al (2016), the stress-strain relations for an isotropic poroelastic material take the form

$$\begin{aligned} \sigma_{ij} &= (\lambda\, e+Q\,\varepsilon)\,\delta_{ij}+2\mu_c\, e_{ij}\,, \quad i,j=\{x,z\}\,,\\ s &= Q\,e+R\,\varepsilon\,, \end{aligned}$$

where δ_{ij} is the Kronecker delta, λ and μ_c are the Lamé coefficients associated with the solid component, Q measures the coupling of changes in the volume of the solid and fluid parts, and R is a parameter measuring the pressure required to force a certain volume of fluid into the pores. These quantities are calculated from measured or estimated values of parameters given in Table 1 using the following formulas

$$\begin{aligned} \lambda &= K_c-\frac{2}{3}\mu_c+\frac{\left[(1-\beta)K_s-K_c\right]^2}{D-K_c}\,,\\ Q &= \frac{\beta K_s\left[(1-\beta)K_s-K_c\right]}{D-K_c}\,,\\ R &= \frac{\beta^2K_s^2}{D-K_c}\,, \end{aligned}$$

where

$$\begin{aligned} D &= K_s\left[1+\beta\left(\frac{K_s}{K_f}-1\right)\right]\,,\\ K_s &= \frac{2\mu\,(1+\nu)}{3\,(1-2\nu)}\,, \end{aligned}$$

and β represents porosity, i.e. the fluid fraction per unit volume. The bulk and shear moduli, K_c and μ_c, are often given imaginary parts to account for viscous effects (Chen et al, 2018). The bulk modulus may be estimated by

$$K_c = \frac{2\mu_c\,(1+\nu)}{3\,(1-2\nu)}(1-\beta)^n\,,$$

where $n=1.42$ and μ_c denotes the complex Voigt shear modulus as defined by

$$\mu_c = \mu - \mathrm{i}\omega\rho_s\eta\,.$$

Note that the porosity is a dimensionless parameter whose range is $\beta\in[0,1]$, taking the limiting value $\beta=0$ for a solid state and $\beta=1$ for a fluid state. In the present physical context, its complement $1-\beta$ may be viewed as a measure of ice concentration in the ice field.

The total effective stress acting at any point in this poroelastic material can thus be expressed as

$$\tau_{ij} = \sigma_{ij} + s\,\delta_{ij}\,, \tag{4}$$

It can be checked that, as $\beta\to 0$ (assuming K_c and μ_c are real), Eq. (4) simplifies to

$$\tau_{ij} = \left(K_s-\frac{2}{3}\mu\right)e\,\delta_{ij}+2\mu\,e_{ij}\,,$$

which is the typical stress-strain relation for an isotropic elastic material. Having the MIZ in mind, this limiting case would correspond to a solid ice pack. On the other hand, as $\beta\to 1$, Eq. (4) reduces to

$$\tau_{ij} = \left(K_f\,\varepsilon-\frac{2}{3}\mu\,e\right)\delta_{ij}+2\mu\,e_{ij}\,,$$

which involves the fluid dilatation ε together with K_f while K_s is absent. The presence of additional terms containing the solid strain tensor (associated with the parameter μ) suggests that this fluid limit, rather than being equivalent to the open ocean, is closer to a situation with a "soft" ice cover such as brash or grease ice, as it may occur near the MIZ border with the open ocean.

Equations of Motion

Taking into account effects of gravity $\mathbf{g}=(0,-g)$, Biot's equations of motion for the ice layer are

$$\begin{aligned} \mu_c\nabla^2\mathbf{u}+\nabla\left[(\lambda+\mu_c)\,e+Q\,\varepsilon\right]+\mathbf{F}_s &= \partial_t^2(\rho_{11}\mathbf{u}+\rho_{12}\mathbf{U})+b\,\partial_t(\mathbf{u}-\mathbf{U})\,,\\ \nabla(Q\,e+R\,\varepsilon)+\mathbf{F}_f &= \partial_t^2(\rho_{12}\mathbf{u}+\rho_{22}\mathbf{U})-b\,\partial_t(\mathbf{u}-\mathbf{U})\,, \end{aligned}$$

symbol	parameter	units
ρ_f	density of pore fluid	kg m^{-3}
ρ_s	density of solid frame	kg m^{-3}
K_f	bulk modulus of pore fluid	Pa
K_s	bulk modulus of solid frame	Pa
K_c	complex bulk modulus	Pa
μ_c	complex shear modulus	Pa
η	kinematic viscosity of pore fluid	m^2 s^{-1}
K_p	permeability	m^2
ω	angular frequency	s^{-1}
ν	Poisson's ratio	
β	porosity	
α	pore tortuosity	

Table 1: Parameters in Biot's equations.

where

$$\begin{aligned}\mathbf{F}_s &= (1-\beta)\rho_s\mathbf{g},\\ \mathbf{F}_f &= \beta\rho_f\mathbf{g}.\end{aligned}$$

The parameter b is a damping parameter to account for friction due to the relative motion between the fluid and the solid constituents. It is related to Darcy's coefficient of permeability K_p by

$$b = \frac{\rho_s\eta\beta^2}{K_p}.$$

In these equations, ρ_{11} and ρ_{22} are density parameters for the solid and fluid parts, and ρ_{12} is a density coupling parameter with a negative value. These are calculated from the following formulas

$$\begin{aligned}\rho_{11} &= (1-\beta)\rho_s - \rho_{12},\\ \rho_{22} &= \beta\rho_f - \rho_{12},\\ \rho_{12} &= \beta(1-\alpha)\rho_f,\end{aligned}$$

where α is a measure of pore tortuosity in the ice layer.

Following Stoll and Kan (1981), we now make the change of variables

$$u = \partial_x\Phi_s - \partial_z\Psi_s, \quad v = \partial_z\Phi_s + \partial_x\Psi_s,$$

$$U = \partial_x\Phi_f - \partial_z\Psi_f, \quad V = \partial_z\Phi_f + \partial_x\Psi_f,$$

in terms of displacement potentials (Φ_s,Φ_f) for the irrotational part and (Ψ_s,Ψ_f) for the rotational part. The above equations of motion can then be rewritten as

$$\begin{aligned}(\lambda+2\mu_c)\nabla^2\Phi_s + Q\nabla^2\Phi_f &= \partial_t^2(\rho_{11}\Phi_s+\rho_{12}\Phi_f) + b\,\partial_t(\Phi_s-\Phi_f),\\ Q\nabla^2\Phi_s + R\nabla^2\Phi_f &= \partial_t^2(\rho_{12}\Phi_s+\rho_{22}\Phi_f) - b\,\partial_t(\Phi_s-\Phi_f),\end{aligned}$$

and

$$\begin{aligned}\mu_c\nabla^2\Psi_s &= \partial_t^2(\rho_{11}\Psi_s+\rho_{12}\Psi_f) + b\,\partial_t(\Psi_s-\Psi_f),\\ 0 &= \partial_t^2(\rho_{12}\Psi_s+\rho_{22}\Psi_f) - b\,\partial_t(\Psi_s-\Psi_f).\end{aligned}$$

Assuming traveling wave solutions of the form

$$(\Phi_s,\Phi_f,\Psi_s,\Psi_f) = [\phi_s(z),\phi_f(z),\psi_s(z),\psi_f(z)]e^{\mathrm{i}(\kappa x-\omega t)},$$

where $\omega\in\mathbb{R}_+$ is the angular frequency and $\kappa = k+\mathrm{i}\,q$, with $k\in\mathbb{R}_+$ being the wavenumber and $q\in\mathbb{R}_+$ the attenuation rate, this leads to a system of 4th-order ordinary differential equations that can be solved analytically, namely

$$\begin{aligned}\phi_s(z) &= C_1F_5\cosh(D_1z)+C_2F_5\sinh(D_1z)\\ &\quad +C_3F_6\cosh(D_2z)+C_4F_6\sinh(D_2z),\\ \phi_f(z) &= C_1F_7\cosh(D_1z)+C_2F_7\sinh(D_1z)\\ &\quad +C_3F_8\cosh(D_2z)+C_4F_8\sinh(D_2z),\end{aligned}$$

and

$$\begin{aligned}\psi_s(z) &= C_5\cosh(D_3z)+C_6\sinh(D_3z),\\ \psi_f(z) &= C_5F_9\cosh(D_3z)+C_6F_9\sinh(D_3z).\end{aligned}$$

Similarly, seeking traveling wave solutions of the form

$$\Phi(x,z,t) = \phi(z)e^{\mathrm{i}(\kappa x-\omega t)},$$

for Eq. (1) in the ocean, we obtain

$$\phi(z) = C_7\cosh(D_4z)+C_8\sinh(D_4z).$$

More details on the constants $D_i\,(i=1,\ldots,4)$ and $F_j\,(j=5,\ldots,8)$ can be found in Chen et al (2019).

Coupling Boundary Conditions

The traveling wave solutions of this coupled system are given in terms of eight coefficients $C_i\,(i=1,2,\ldots,8)$, so eight boundary conditions are needed in order to close it. These boundaries include the air-ice interface at $z=h$, the ice-water interface at $z=0$ and the ocean floor at $z=-H$, where different boundary conditions are specified. In particular, because water in the ocean is taken to be inviscid, it does not exert any tangential stress on the ice layer. On the other hand, Bernoulli's condition at the ice-water interface implies that the ice normal stress should match the water pressure.

Let $\eta_2(x,t)=\eta_1(x,t)+h$ denote the vertical displacement of the top boundary of the ice layer relative to $z=0$. We impose:

- at the air-ice interface $z=h$
  1. vanishing of tangential stress
  $$\partial_z u+\partial_x v = 0,$$
  2. vanishing of solid normal stress
  $$\lambda\,e+Q\,\varepsilon+2\mu_c\,e_{zz}+(1-\beta)\rho_s g\,\eta_2 = 0,$$
  3. vanishing of fluid normal stress
  $$Q\,e+R\,\varepsilon+\beta\rho_f g\,\eta_2 = 0,$$
- at the ice-water interface $z=0$
  4. continuity of vertical displacement
  $$(1-\beta)\,v+\beta\,V = \eta_1,$$
  5. vanishing of tangential stress
  $$\partial_z u+\partial_x v = 0,$$
  6. continuity of solid normal stress
  $$\lambda\,e+Q\,\varepsilon+2\mu_c\,e_{zz}+(1-\beta)\rho_s g\,\eta_1 = -(1-\beta)P,$$

7. continuity of fluid normal stress

$$Qe + R\varepsilon + \beta\rho_f g\,\eta_1 = -\beta P\,,$$

- at the ocean floor $z = -H$

8. vanishing of fluid flux

$$\partial_z \Phi = 0\,.$$

This system of equations is completed by the kinematic condition (2), which gives η_1 (and thus η_2) from Φ, and by Bernoulli's condition (3), which gives P at the ice-water interface.

More explicitly, in terms of the potentials for traveling wave solutions, these boundary conditions read:

- at the air-ice interface $z = h$

$$\begin{aligned}
(\mathrm{i}\kappa\phi_s - \psi_s')' + \mathrm{i}\kappa(\phi_s' + \mathrm{i}\kappa\psi_s) &= 0\,,\\
-\mathrm{i}\omega\left[\lambda\nabla^2\phi_s + Q\nabla^2\phi_f + 2\mu_c(\phi_s' + \mathrm{i}\kappa\psi_s)'\right] + (1-\beta)\rho_s g\,\phi' &= 0\,,\\
-\mathrm{i}\omega(Q\nabla^2\phi_s + R\nabla^2\phi_f) + \beta\rho_f g\,\phi' &= 0\,,
\end{aligned}$$

- at the ice-water interface $z = 0$

$$\begin{aligned}
-\mathrm{i}\omega\left[(1-\beta)(\phi_s' + \mathrm{i}\kappa\psi_s) + \beta(\phi_f' + \mathrm{i}\kappa\psi_f)\right] - \phi' &= 0\,,\\
(\mathrm{i}\kappa\phi_s - \psi_s')' + \mathrm{i}\kappa(\phi_s' + \mathrm{i}\kappa\psi_s) &= 0\,,\\
-\mathrm{i}\omega\left[\lambda\nabla^2\phi_s + Q\nabla^2\phi_f + 2\mu_c(\phi_s' + \mathrm{i}\kappa\psi_s)'\right] & \\
+(1-\beta)\rho_s g\,\phi' - (1-\beta)\rho_f(-\omega^2\phi + g\,\phi') &= 0\,,\\
-\mathrm{i}\omega(Q\nabla^2\phi_s + R\nabla^2\phi_f) + \beta\rho_f g\,\phi' - \beta\rho_f(-\omega^2\phi + g\,\phi') &= 0\,,
\end{aligned}$$

- at the ocean floor $z = -H$

$$\phi' = 0\,.$$

The primes denote differentiation with respect to z and the Laplacian operator reduces to

$$\nabla^2 = -\kappa^2 + \partial_z^2\,.$$

Note that any constant term in conditions 1∼8 may be eliminated by taking the time derivative of these equations. This amounts to multiplying the remaining terms by a common coefficient $-\mathrm{i}\omega$ which may then be factored and canceled out.

DISPERSION RELATION

The resulting linear system admits eight unknowns $C_i\,(i = 1,\ldots,8)$. By enforcing the determinant of the associated 8×8 coefficient matrix to be zero for nontrivial solutions and with help from the software Mathematica, we obtain an exact dispersion relation that can be stated as

$$\omega^2 = \left(\frac{T_1 + g\,T_2}{T_3}\right) D_4 \tanh(D_4 H)\,. \tag{5}$$

The lengthy expressions of T_1, T_2 and T_3 can be found in Chen et al (2019). Note that the right-hand side of (5) depends on κ but is also a function of ω.

For a given value of ω and other parameter values, this dispersion relation is solved numerically for κ using the root-finding routine *fsolve* in Matlab. More specifically, as κ is generally complex, Eq. (5) is split up into its real and imaginary parts. This leads to a system of two independent equations that are solved simultaneously for the two unknowns k and q. As pointed out in Mosig et al (2015) and Zhao et al (2017), such a dispersion relation very likely admits multiple possible roots for k and

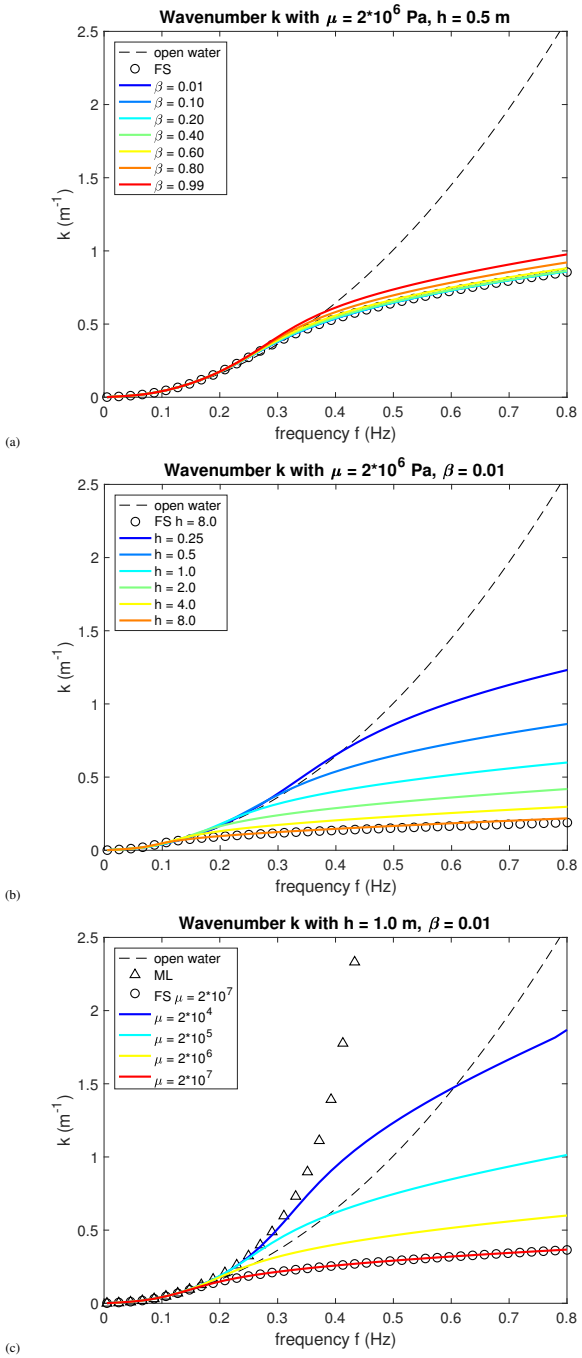

Fig. 2: Wavenumber k vs. frequency f for (a) varying porosity β, (b) varying ice thickness h and (c) varying shear modulus μ, in the porous elastic case ($\eta = 0$). Open-water, FS and ML predictions are shown for comparison.

q. Therefore, as suggested by WS, we adopt the following criteria to select relevant solutions: (i) k is the wavenumber closest to the open-water value k_0 and (ii) q is the lowest possible attenuation rate. That is, given ω, we solve (5) for κ such that the error $|\kappa - (k_0 + \mathrm{i}0)|$ is smallest. The open-water wavenumber k_0 satisfies the standard dispersion relation

$$\omega^2 = gk\tanh(kH)\,,$$

for surface gravity waves and is also determined numerically.

Typical parameter values for sea ice that we specify in the computations are (in SI units, see Table 1): $g = 9.81$, $\rho_s = 917$, $\rho_f = 1025$, $c = 1449$, $\alpha = 5$, $\nu = 0.3$, $\mu = 2 \times 10^6$, and accordingly $K_s = 4.3 \times 10^6$, $K_f = K_s/4 = 1.1 \times 10^6$ (Williams and Francois, 1992). We choose $H = 100$ m unless stated otherwise. Because of the large disparity in orders of magnitude among the various parameters, we find it convenient to non-dimensionalize the equations by using H as a characteristic length scale, $\sqrt{H/g}$ as a characteristic time scale and $\rho_f H^3$ as a characteristic mass. In the following tests, we examine predictions from (5) by varying β and other parameters, and compare them to results obtained from simpler existing models. Although we allow $\beta \neq 0$, we only investigate the frictionless case in this preliminary study by setting $b = 0$.

Porous Elastic Case

A porous elastic model is obtained if μ_c and K_c are taken to be real (i.e. $\eta = 0$, no viscosity), and accordingly all roots κ of (5) are real. Numerical estimates of wavenumber k versus frequency $f = 2\pi\omega$ are presented in Fig. 2 for varying β, h and μ. On each plot, FS results are included for comparison and open-water results are also shown as a reference.

Figure 2(a) illustrates porosity effects, with $\mu = 2 \times 10^6$ Pa, $h = 0.5$ m and β ranging from 0.01 to 0.99. Recall that the porosity parameter β controls the type of ice cover: lower β represents a more compact ice layer, while higher β indicates a sparser ice layer. As expected, for very low porosities, our curves are close to FS. For higher porosity, dispersive effects become weaker. Given f, the higher the porosity, the larger the wavenumber (which corresponds to shorter wavelength). Figure 2(b) examines (5) for low porosity ($\beta = 0.01$) and varying h. This case is similar to the FS model. As the ice thickness shrinks (i.e. as h gets smaller), the wavenumber gets closer to the open-water value. Figure 2(c) shows elasticity effects for $\beta = 0.01$ and $h = 1$ m, considering values of μ with various orders of magnitude. Shear modulus μ is a measure of the material rigidity, therefore higher μ is indicative of a stiffer ice cover. For comparison, predictions based on the ML model (which ignores the elastic response of the ice layer) are also included on this plot. As expected, for small μ, our curves are close to ML.

Porous Viscous Elastic Case

If viscosity is taken into account by allowing μ_c and K_c to be complex with imaginary parts, then Eq. (5) describes a porous viscous elastic ice layer floating on a slightly compressible ocean. Accordingly, the roots κ of (5) are complex, yielding values for the wavenumber k and the attenuation rate q. Similar to the previous case, we conduct several tests by varying β, h as well as the viscosity parameter η, as presented in Figs. 3∼5. Shear modulus is taken to be $\mu = 2 \times 10^6$ Pa in all these tests. Each plot includes comparison with open-water, EFS and WS results. Note that, although both EFS and WS models feature viscoelasticity, the EFS model is based on thin plate theory while the WS model describes the ice cover as a distinctive separate layer above the ocean (as in the present formulation).

Figure 3 shows results for $h = 1$ m, $\eta = 10^{-2}$ m^2 s^{-1} and varying β. For low porosities, we see no much difference in wavenumber between our results and the EFS/WS predictions; all these curves pretty much coincide. Dispersive effects however strengthen in the open-water limit and, accordingly, our results become slightly more distinctive (with larger k) at higher porosities. We also observe stronger attenuation, compared to EFS/WS, in this limit, and it is more pronounced at higher frequencies. More specifically, our predictions on q are almost identical to

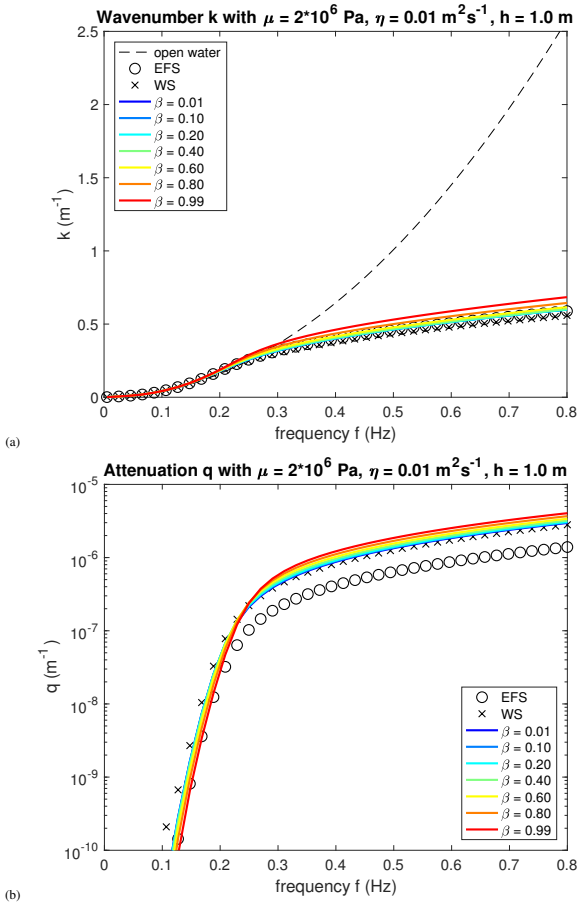

Fig. 3: (a) Wavenumber k and (b) attenuation rate q vs. frequency f for varying porosity β in the porous viscous elastic case. Open-water, EFS and WS predictions are shown for comparison.

WS for low β but yield slightly larger values at higher β. The EFS values on the other hand remain visibly lower. Overall, both k and q increase as f increases, which gives a natural correspondence between spatial and temporal scales. This is also consistent with the intuition that viscosity tends to be stronger at smaller scales and thus shorter waves are more damped.

In Fig. 4, we set $\beta = 0.3$ and $\eta = 10^{-1}$ m^2 s^{-1} but vary h. The wavenumber curves in Fig. 4(a) look similar to those in Fig. 2(b) for the porous elastic case, showing convergence to the open-water limit as $h \to 0$. We again see a close match with EFS and WS. Figure 4(b) depicts the corresponding graphs of attenuation rate and reveals differences in their slope at low frequencies as h is varied. We note incidentally that, although q grows monotonically with f, its slope is not a monotonic function of f. This behavior is also observed for k but is more apparent on graphs of q. The slight inflection point at $f \simeq 0.3$ Hz on the wavenumber curves (see also Fig. 2c), which coincides with a sharp change of slope on the attenuation curves, corresponds to the transition from mass loading to flexural rigidity as a dominant effect (Collins et al, 2017). Past this transition, the fact that short waves experience more attenuation in thinner ice (which is rather counter intuitive) is reminiscent of a common feature in models for water waves over seabed composed of a viscous mud layer, where dissipation has a non-monotonic dependence on mud-layer thickness, with thicker layers being less dissipative (Dalrymple and Liu, 1978).

Figure 5 shows graphs of k and q for $\beta = 0.3$, $h = 3$ m and varying

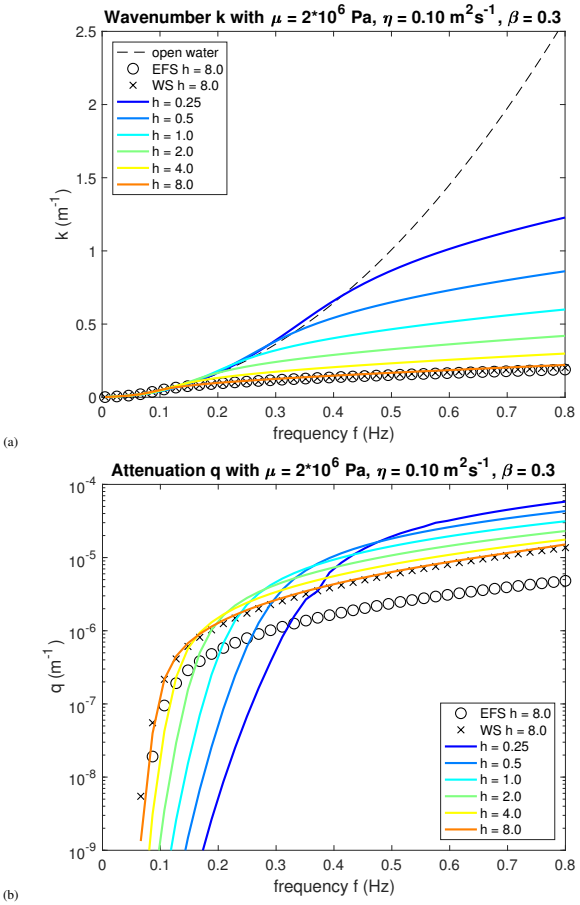

Fig. 4: (a) Wavenumber k and (b) attenuation rate q vs. frequency f for varying ice thickness h in the porous viscous elastic case. Open-water, EFS and WS predictions are shown for comparison.

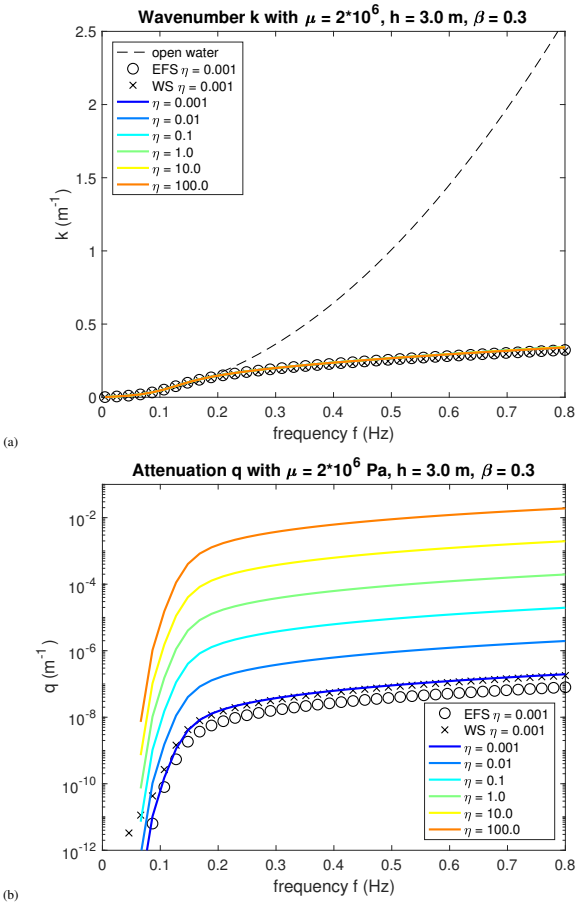

Fig. 5: (a) Wavenumber k and (b) attenuation rate q vs. frequency f for varying viscosity η in the porous viscous elastic case. Open-water, EFS and WS predictions are shown for comparison.

η. This test confirms that viscosity has no effect on k, only on q. The wavenumbers are found to all lie on the same curve. On the other hand, the larger the viscosity, the stronger the attenuation at any frequency. This dependence of q on η seems to be uniform in the sense that the attenuation curves retain the same shape and are simply shifted upward as η increases. Further comparison with EFS/WS is provided in Fig. 5 and displays the same features as noticed in the two previous figures.

COMPARISON WITH EXPERIMENTAL DATA

In this section, we provide preliminary validation of our poroelastic model against laboratory experiments by Newyear and Martin (1997). These authors conducted experiments using a wave tank located in a laboratory cold room and investigated wave propagation in grease ice.

Comparison between their measurements of k and q, and our model predictions, is given in Fig. 6 for $\beta = 0.52$, $h = 0.146$ m, $H = 0.354$ m, $\mu = 2 \times 10^3$ Pa and $\eta = 1.8$ m^2 s^{-1}. The values of β, h and H were inferred from these authors' paper, while the values of μ and η were adjusted in order to obtain a close match with their measurements. Overall, the general trend of these experimental data is well captured by our numerical results. The agreement on k is especially good. Our computations however undershoot the measurements of attenuation rate at high frequencies. The rapid increase of q with f, as indicated in Fig. 6(b), is characteristic of wave propagation in grease ice, which is known to be dominated by viscous effects (de Carolis and Desiderio, 2002). Further investigation is needed here and is left for future work.

CONCLUSIONS

We have proposed a two-dimensional continuum model for linear wave propagation in ice-infested seas. It is based on a two-layer formulation where the floating sea ice is described as a homogeneous poroelastic material according to Biot's theory, and the underlying ocean is viewed as a slightly compressible fluid. Viscoelasticity can also be included in this formulation by allowing elasticity parameters to be complex numbers. In view are potential applications to modeling wave scattering and attenuation in the MIZ. A parameter of special interest in our wave-ice model is the porosity, whose complement may serve as a measure of ice concentration in the ice field.

We have derived the exact dispersion relation for traveling wave solutions of this coupled system and obtained numerical estimates for its complex roots. These represent the wavenumber and attenuation rate associated with the traveling waves. We have conducted several tests to examine the dependence of results on various parameters, and performed comparisons with other models (including the FS, EFS and WS models). We have also validated our model predictions against laboratory measurements of wave propagation in grease ice and found satisfactory agreement.

Further validation against experimental data is needed and this is

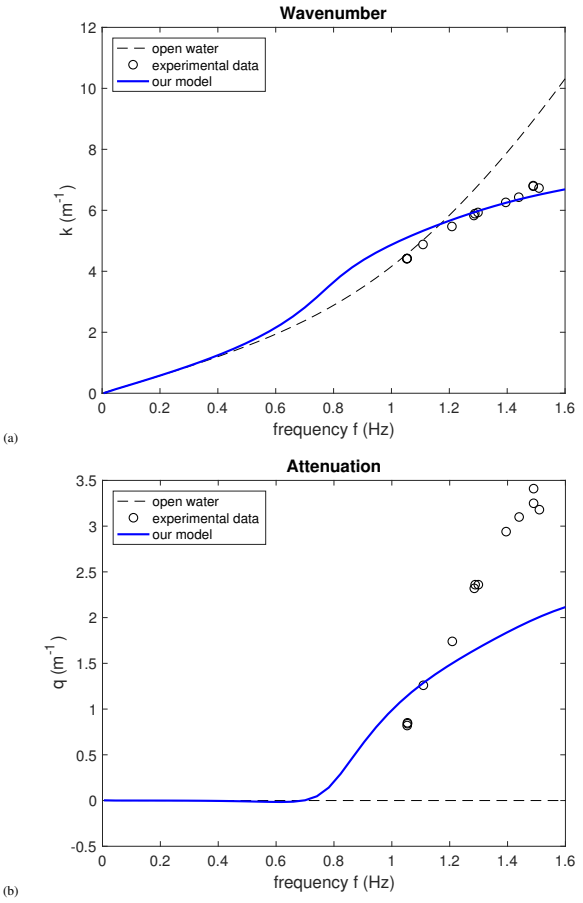

Fig. 6: (a) Wavenumber k and (b) attenuation rate q vs. frequency f for $\beta = 0.52$, $h = 0.146$ m, $H = 0.354$ m, $\mu = 2 \times 10^3$ Pa and $\eta = 1.8$ m^2 s^{-1} in the porous viscous elastic case. Open-water predictions and experimental data from Newyear and Martin (1997) are shown for comparison.

envisioned for future work (Doble et al, 2015). It would also be of interest to investigate nonlinear extensions of this poroelastic formulation. Nonlinear theory of wave-ice interactions has received increasing attention in recent years (Guyenne and Părău, 2012, 2014, 2017).

ACKNOWLEDGEMENTS

This work is partially supported by the NSF through grant number DMS-1615480. P. Guyenne also thanks the Tsinghua Sanya International Mathematics Forum (China) for its hospitality during a visit in the winter 2019.

REFERENCES

Biot, MA (1956). "Theory of propogation of elastic waves in a fluid-saturated porous solid. I. lower frequency range," *J Acoust Soc Amer*, 28, 168-178.

Biot, MA (1956). "Theory of propagation of elastic waves in a fluid-saturated porous solid. II. Higher frequency range," *J Acoust Soc Amer*, 28, 179-191.

Chen, H, Gilbert, RP, and Guyenne, P (2018). "A Biot model for the determination of material parameters of cancellous bone from acoustic measurements," *Inverse Problems*, 34, 085009.

Chen, H, Gilbert, RP, and Guyenne, P (2019). "Dispersion and attenuation in a porous viscoelastic model for gravity waves on an ice-covered ocean," *Submitted*.

Collins III, CO, Rogers, WE, and Lund, B (2017). "An investigation into the dispersion of ocean surface waves in sea ice," *Ocean Dyn*, 67, 263-280.

Dalrymple, RA, and Liu, PL-F (1978). "Waves over soft muds: a two-layer fluid model," *J Phys Oceanogr*, 8, 1121-1131.

de Carolis, G, and Desiderio, D (2002). "Dispersion and attenuation of gravity waves in ice: A two-layer viscous fluid model with experimental data validation," *Phys Lett A*, 305, 399-412.

Doble, MJ, de Carolis, G, Meylan, MH, Bidlot, J-R, and Wadhams, P (2015). "Relating wave attenuation to pancake ice thickness, using field measurements and model results," *Geophys Res Lett*, 42, 4473-4481.

Fox, C, and Squire, VA (1994). "On the oblique reflexion and transmission of ocean waves at shore fast sea ice," *Phil Trans R Soc Lond A*, 347, 185-218.

Gilbert, RP, Guyenne, P, and Shoushani, M (2016). "Recovery of parameters of cancellous bone by acoustic interrogation," *Inv Probl Sci Engng*, 24, 284-316.

Guyenne, P, and Părău, EI (2012). "Computations of fully nonlinear hydroelastic solitary waves on deep water," *J Fluid Mech*, 713, 307-329.

Guyenne, P, and Părău, EI (2014). "Finite-depth effects on solitary waves in a floating ice sheet," *J Fluids Struct*, 49, 242-262.

Guyenne, P, and Părău, EI (2017). "Numerical study of solitary wave attenuation in a fragmented ice sheet," *Phys Rev Fluids*, 2, 034002.

Keller, JB (1998). "Gravity waves on ice-covered water," *J Geophys Res*, 103, 7663-7669.

Kohout, AL, and Meylan, MH (2008). "An elastic plate model for wave attenuation and ice floe breaking in the marginal ice zone," *J Geophys Res*, 113, C09016.

Mosig, JE, Montiel, F, and Squire, VA (2015). "Comparison of viscoelastic type models for ocean wave attenuation in ice-covered seas," *J Geophys Res*, 120, 6072-6090.

Newyear, K, and Martin, S (1997). "A comparison of theory and laboratory measurements of wave propagation and attenuation in grease ice," *J Geophys Res*, 102, 25091-25099.

Renzi, E, and Dias, F (2014). "Hydro-acoustic precursors of gravity waves generated by surface pressure disturbances localised in space and time," *J Fluid Mech*, 754, 250-262.

Squire, VA (2007). "Of ocean waves and sea-ice revisited," *Cold Reg Sci Tech*, 49, 110-133.

Stoll, RD, and Kan, TK (1981). "Reflection of acoustic waves at a water-sediment interface," *J Acoust Soc Amer*, 70, 149-156.

Wadhams, P, Squire, VA, Goodman, DJ, Cowan, AM, and Moore, SC (1988). "The attenuation rates of ocean waves in the marginal ice zone," *J Geophys Res*, 93, 6799-6818.

Wang, R, and Shen, HH (2010). "Gravity waves propagating into an ice-covered ocean: A viscoelastic model," *J Geophys Res*, 115, C06024.

Williams, KL, and Francois, RE (1992). "Sea ice elastic moduli: Determination of Biot parameters using in-field velocity measurements," *J Acoust Soc Amer*, 91, 2627-2636.

Zhao, X, Cheng, S, and Shen, HH (2017). "Nature of wave modes in a coupled viscoelastic layer over water," *J Engng Mech*, 143, 04017114.